Cell Reports, Volume *19*

Supplemental Information

Cellular Decision Making by Non-Integrative Processing of TLR Inputs

Ryan A. Kellogg, Chengzhe Tian, Martin Etzrodt, and Savaş Tay

1. Classifier

Description of Classifiers

We construct one classifier for every input condition, and the primary objective of this classifier is to determine whether a cellular response under co-stimulation is a more LPS-like, PAM-like or mixed response (if exist). For the input condition of LPS dose x and PAM dose y, the training data for the classifier are the time series of nuclear NF-κB concentrations under only LPS dose x challenge or only PAM dose y challenge, and the test data are the time series under LPS dose x and PAM dose y co-stimulation. We obtain around 100-200 cellular responses from the experiments, and we only use active trajectories for training and testing. Our experiments show that the fractions of active cells are 95% for LPS 100 ng/mL, 73% for LPS 33 ng/mL, 47% for LPS 11 ng/mL and 100% for all other inputs. The size of training data therefore varies between 100 and 300 cells and the size of test data is around 100-200 for all input conditions. For classification of model-simulated time courses, the training data consist of at most 500 LPS-type (only active time courses are considered) and 500 PAM-type and the size of the test data is 500.

To determine the potential mixed-response, we employ a two-step procedure for classification. The first step is to construct individual classifiers to classify a test cellular response into more LPS-like or more PAM-like. We use bootstrap to diversify the training data for individual classifiers. The second step is to aggregate all outputs from the individual classifiers based on majority-vote: if more than ν fraction of outputs gives LPS-like (PAM-like), we claim the test data is LPS-like (PAM-like); if the fraction of neither LPS outputs nor PAM outputs reaches ν, this test data is considered uncertain and we interpret this data as the mixed type.

We notice that constructing individual classifiers based on explicit features could limit the performance in identifying mixed responses. The reason is that classifiers trained on explicit features will only evaluate the test data from pre-defined perspectives, and these perspectives may contain a bias on one of the two labels. To eliminate bias, we choose to employ a data-driven approach and allow classification algorithms to automatically determine the features that show the best separation of training data. In this work we use decision tree models to achieve this objective. A decision tree model contains many splits and each split represents a YES-NO question, and the classification outcome is determined by the answers to a series of YES-NO questions. The splits are determined by the algorithm such that the labels of resulting two groups (those answering YES and those answering NO) are as homogeneous as possible (minimizing Gini index). Due to the bootstrapping feature, we allow the decision trees to evaluate the test data from diverse perspectives. By definition, our classifier belongs to a bagging classifier.

One limitation of our data-driven approach is that some splits in the individual decision tree models may be induced by the noise in the data, rather than the difference between the LPS- and PAM-like cellular responses. These decision trees may give wrong classification results and individual decision tree models may not achieve a high level of agreement on apparent LPS- or PAM-like test data. Consequently, we should not choose the value of the threshold ν to be very high. In principle, we may increase the value of ν by increasing the size of the training data.

Selection of Parameters

We evaluate our classifier by cross-validation and we choose the values of two unknown parameters (number of decision trees N and the threshold ν) by maximizing the accuracy. To be precise, for each combination of N and ν, we train a bagging classifier for every input condition and compute the fractions that the classifier outputs a correct label ("correct"), an incorrect label ("incorrect") or an uncertain label ("uncertain") by 10-fold cross-validation. The overall accuracy of classifiers with (N, ν) is defined as the average value of the "correct" fractions of all nine input conditions.

We sample the values of N and ν in a wide range and the accuracies are shown in Table S1. We observe that the accuracy of the bagging classifiers is not strongly affected by the number of decision trees (N) except for very high thresholds (ν), and that the accuracy decreases as the threshold values (ν) increases. We then choose N=50 and restrict our attention to the input condition of our primary interest (LPS 11 ng/mL, PAM 4.4 ng/mL). We find that the primary cause for the reduction in the accuracy of the bagging classifier with higher ν is the uncertain labels (Figure S1A), and this finding holds for all other input conditions (Figure S1B).

Based on the parameter sampling, we choose N=50, ν=0.6 to be the optimal parameter values. We notice that ν=0.6 also maximizes the fraction of incorrect labels, though this fraction is small. The resulting classifier has an average accuracy of 89% and an accuracy of at least 85% for every input condition (Table S1 and S2).

Example Decision Tree

An example decision tree for LPS 11 ng/mL and 4.4 ng/mL and its relevant statistics are shown in Figure S1C and Table S3. The importance is defined as the increase in node purity (how uniform the labels are) after split, and is computed with matlab command predictorImportance. The first two predictors of the tree, c(181) and c(228), evaluate the nuclear NF-κB activities around 3 and 4 hours after stimulation. The decision tree is likely to classify trajectories with high values as PAM responses. The last two predictors, c(50) and c(16), evaluate the early NF-κB activities and trajectories with high values are classified as LPS responses. This decision tree is consistent with the fact that LPS induces a rapid, short response while PAM induces a delayed but sustained response.

Classification with Threshold ν=0.8

To further justify our choice for parameter values, we train classifiers with parameter values N=50, ν=0.8 and repeat the classification figures in the main text (Figure 3D, Figure 4B-C), as shown in Figure S1F-G. We restrict our attention to mid/low doses of LPS and PAM to allow a sufficient difference between LPS-like and PAM-like responses. We show that no more than 10% of simulated cellular responses are determined to be mixed type (Figure S1F). For experimental cellular responses, our classifier predicts a substantially higher percentage of mixed type responses (20%-30%). Despite these high numbers, we argue that our main conclusion that cells process competing TLR ligands in a non-integrative

fashion still holds. Firstly, the percentage 20%-30% is still well below 50%, indicating that the majority of responses are still either LPS- or PAM-like. Secondly, the accuracy of the bagging classifier with ν=0.8 is lower compared with the ones with lower threshold values. Figure S1B shows that when applied to training data, the classifier with ν=0.8 outputs around 20% of mixed output, and we should take this number into account when interpreting the percentages in Figure S1G. Here we consider the differences between the percentages in Figure S1G (classifier's outputs for the test data) and 20% (classifier's outputs for the training data) to be a more realistic description of the actual percentage of mixed-type responses, which are around 10%, indicating that the mixed responses are a minority. In summary, we claim that our main conclusion is unaffected with a higher value of threshold ν.

Classification of artificially generated "mixed" time courses

To evaluate the quality of our classifier in identification of mixed responses, we restrict to the low doses and create 1000 artificial "mixed" time courses by adding one randomly selected LPS-training trajectory and one randomly selected PAM-training trajectory. We then apply our classifier to these artificial data and plot the result in Figure S1D-E. Indeed, most artificial data are classified as mixed. If these artificial trajectories accurately reflect the reality, this analysis suggests that our classifier fails to identify around 40% mixed responses for this dose combination. The corrected fraction of mixed responses should be 10% (reported by classifier) divided by 60%, which equals to 16%. This is still a small number and we claim that our conclusion remains valid.

2. Mathematical Model of Competing TLR Ligands

We construct a mathematical model for competing TLR ligands by extending our previously published models of TNF and LPS pathways (Kellogg et al., 2015, Tay et al., 2010). All reactions are modeled using the mass action law. Activation and inactivation are modeled using Michaelis-Menten terms or Hill terms, if cooperativity exists. In this work, rather than fitting to experimental cellular responses precisely, our emphasis is to use mathematical models to illustrate the possibility that an ultrasensitive negative feedback and endosomal signaling can mediate non-integrative processing of competing ligands, and our model only needs to capture the main features of LPS and PAM cellular responses. For this reason, we put strong constraints to our models. We assume that the overall signaling network topology for both TLR4- and TLR2-mediated signaling is identical, and that the parameter values below TRAF6 are identical for both signaling pathways. This allows us to treat distinct signal inputs with reduced model complexity and to attribute the differences between the two pathways to the receptor-level parameter values. We also exclude intrinsic noises and only consider receptor-level extrinsic noise (total number of TLR4 and TLR2 follow lognormal distributions), so our simulated cellular responses are expected to be more "ordered" than the experiments.

Conversion from Concentration to Molecular Numbers

The microfluidics platform utilized in this study contains chambers of size 1.12 mm*0.9 mm*0.040 mm (Kellogg et al., 2014, Gómez-Sjöberg et al., 2007) and each chamber contains around 100 cells. The molecular weight of LPS is set to

10kDa (Sigma-Aldrich, 2008) and the molecular weight of Pam_3CSK_4 is 1509.6 Da (Invivogen). We then conclude that 1 ng/mL LPS input gives that every cell interacts with $2.4*10^4$ ligands, and 1 ng/mL PAM input gives $1.6*10^5$ ligands per cell.

Structure of the ODE Model

Table S4 summarizes the reactions and the mathematical descriptions for the receptor-level signaling. Here we assume that the total number of TLR4 (both in TLR4 and LPS.TLR4 forms) follows a log-normal distribution with parameter μ_l and σ_l, and the total number of TLR2 (both TLR2 and PAM.TLR2) follows a log-normal distribution with parameter μ_p and σ_p. LPS.TLR4 and PAM.TLR2 complexes function in distinct locations (Brandt et al., 2013). To account for this, we model TRAF6 molecules activated by LPS (denoted as TRAF6a(LPS)) and the ones activated by PAM (denoted as TRAF6a(PAM)) separately. Both forms of TRAF6a may activate IKK independently, and we model the reaction of IKK activation ($IKK_n \rightarrow IKK_a$) with rate

$$c_{1(LPS)} \frac{[TRAF6a(LPS)]^4}{[TRAF6a(LPS)]^4+K^4_{TRAF6a(LPS)}} [IKKn] + c_{1(PAM)} \frac{[TRAF6a(PAM)]^4}{[TRAF6a(PAM)]^4+K^4_{TRAF6a(PAM)}} [IKKn].$$

We integrate the transcriptional control of miR-146a in the same fashion as other transcripts, also shown in Table S4.

Parameter Values

To constrain the degrees of freedom in parameter estimation, we adopt the parameter values in TLR4-mediated receptor-level signaling from our previous LPS model (Kellogg et al., 2015), and we only adjust the binding rate between TLR4 and LPS to account for the lower fraction of active cells under ultrapure LPS challenge. We also assume that similar reactions in TLR4- and TLR2 signaling take the same kinetic constants whenever possible. The parameters related to miR-146a are obtained by fitting to the bulk expression data. The parameter values for the receptor-level signaling and the miR-146a are listed in Table S5.

Remarks

- Since our model is not designed to fit to experimental data precisely, we determine the parameter values by manual trial-and-error to avoid the computationally expensive process of parameter estimation.
- We exclude the TRIF-mediated TLR4 pathway from the model as we find that pure LPS has a high degradation rate in the experiments and few NF-κB responses are observed beyond the initial peak. This finding is supported by our previous work that an LPS stimulus without continuous perfusion yields cellular responses mainly with only one peak while a stimulus with perfusion yields sustained oscillation (Kellogg et al., 2015). Moreover, the TRIF pathway is not active in 3T3 cells (Alexander Hoffmann, personal correspondence).
- The mathematical model suggests that the non-integrative processing of LPS and PAM input signals can be explained by the different timescales in receptor-level signaling and the miR-146a negative feedback.

- The endosomal signaling of TLR2 is described by the receptor-level kinetic constants. The low binding rate between PAM and TLR2 (p_b) accounts for both binding and internalization processes. The low unbinding rate (p_f) models internalization as an integrator and allows the endosomal level of PAM.TLR2 to be less sensitive to the degradation of PAM input signal.
- To control the complexity of the model, we model the synthesis and degradation of miR-146a in a similar fashion to our TNF model (Tay et al., 2010). The activation rate of nuclear NF-κB on miR-146a genes is slower than the rates for other genes. This is consistent with miR-146a functioning as a slow feedback (Figure 2).
- miR-146a inhibits signaling by targeting IRAK1/2 and TRAF6 mRNA (Nahid et al., 2011). Here we employ a phenomenological approach by modeling with a Hill term. The Hill coefficient 4 is chosen to account for the ultrasensitivity of the miR-146a negative feedback and can in principle be replaced by other integers greater than 1.
- We notice that the model requires a lower level of TRAF6a (~10^3) than the Hill constant (k_{TRAF6a}, 3.5*10^3) to activate the downstream pathway. The reason is that we assume many parameter values to be identical to the LPS model where this Hill constant does not serve as the threshold due to the NF-κB-level variability. It is worth mentioning that the predictive power of the model is not sacrificed as the cooperativity among TRAF6 in activating IKK is more relevant to digital signaling.
- The model predicts that LPS degradation inhibits NF-κB oscillation after the first peak, without the necessity of miR-146a. This prediction is due to the fact that we use the relevant parameter values from the existing LPS model where miR-146a was not considered. One alternative possibility is that LPS degrades slower and the inhibition of NF-κB oscillation was induced by miR-146a. However, the model maintains its predictive power since LPS activates the cell in a faster timescale than PAM.
- For PAM responses, our model predicts a stronger dependency of the maximal peak amplitudes on the input doses (Figure 1C and S2e). The reason is that we model endosomal signaling of PAM with the mathematical structure of membrane signaling, in order to eliminate several reactions and free parameters (Table S4). Consequently, the endosomal level of PAM.TLR2 complexes reaches the steady state value exponentially in time (Figure 2A). The rate of exponential accumulation and the steady state value are governed by the timescales of low-dose responses (~200 min delay and shut-off at 300-400 min), leaving us little flexibility to tune the dependency of the steady state value (governing the maximal peak amplitude) on the input dose. This issue can be possibly resolved by modeling the endosomal processing in greater details.

Mechanistic difference between LPS and PAM responses

While we argued that NF-kB pathway induces digital signaling in a series of manuscripts (Tay et al., 2010, Kellogg et al., 2015), the pathway has its analog aspect. For example, cells stimulated by a high dose of TNFα generally exhibit a high peak amplitude (Tay et al., 2010). Similar relation can be observed between LPS dose and the expression levels of downstream genes (Kellogg et al., 2015). We capture this analog aspect in the mathematical model. For example, we simulate the model with various constant levels of activated TRAF6 (TRAF6a) and plot the properties of the first NF-

κB peak in Figure S2G. The level of TRAF6a characterizes the level of LPS.TLR4 complexes for LPS stimulation and the level of endosomal PAM.TLR2 complexes for PAM stimulation. We find that a high TRAF6a level, induced by a high dose of LPS/PAM, leads to a faster and stronger response. For all levels, the timescale of NF-κB peaks is 10^1 min.

The time series of NF-κB activities can be determined by comparing the timescales of TRAF6a accumulation and NF-κB peaks. For stimulation with a low dose of PAM, cells accumulate TRAF6a in around 200 min (Figure 2A), which is in a slower timescale compared to NF-κB oscillation. TRAF6a may activate NF-κB before reaching its maximal level and these peaks are of lower amplitudes than the peak induced by TRAF6 at its maximal level. The miR-146a produced during these peaks is not sufficient to block the pathways (notice the Hill term for miR-146a inhibition). Consequently, we may observe an NF-κB oscillation of increasing amplitudes. Meanwhile, for stimulation with a high dose of PAM, the timescale of TRAF6a accumulation equals to the timescale of NF-κB oscillation. The initial peak is triggered when TRAF6a is already around its maximal level and the induced miR-146a rapidly blocks all pathways. Therefore, we observe a single peak response. For LPS stimulation, the initial peak is mediated by MyD88 from the membrane, so there exists no timescale separation and we observe a single peak response.

References

BRANDT, K. J., FICKENTSCHER, C., KRUITHOF, E. K. O. & DE MOERLOOSE, P. 2013. TLR2 Ligands Induce NF-κB Activation from Endosomal Compartments of Human Monocytes. *Plos ONE,* 8**,** e80743.

GÓMEZ-SJÖBERG, R., LEYRAT, A. A., PIRONE, D. M., CHEN, C. S. & QUAKE, S. R. 2007. Versatile, Fully Automated, Microfluidic Cell Culture System. *Analytical Chemistry,* 79**,** 8557-8563.

INVIVOGEN. *Pam3CSK4* [Online]. Available: http://www.invivogen.com/pam3csk4 [Accessed 06.01 2015].

KELLOGG, R. A., GÓMEZ-SJÖBERG, R., LEYRAT, A. A. & TAY, S. 2014. High-throughput microfluidic single-cell analysis pipeline for studies of signaling dynamics. *Nature Protocols,* 9**,** 1713-1726.

KELLOGG, R. A., TIAN, C., LIPNIACKI, T., QUAKE, S. R. & TAY, S. 2015. Digital signaling decouples activation probability and population heterogeneity. *eLife,* 4**,** e08931.

NAHID, M. A., SATOH, M. & CHAN, E. K. L. 2011. MicroRNA in TLR signaling and endotoxin tolerance. *Cellular & Molecular Immunology,* 8**,** 388-403.

SIGMA-ALDRICH 2008. *Lipopolysaccharides,* http://www.sigmaaldrich.com/technical-documents/articles/biology/glycobiology/lipopolysaccharides.html.

TAY, S., HUGHEY, J. J., LEE, T. K., LIPNIACKI, T., QUAKE, S. R. & COVERT, M. W. 2010. Single-cell NF-κB dynamics reveal digital activation and analogue information processing. *Nature,* 466**,** 267-271.

YAO, B., LA, L. B., CHEN, Y.-C., CHANG, L.-J. & CHAN, E. K. L. 2012. Defining a new role of GW182 in maintaining miRNA stability. *EMBO Reports,* 13**,** 1102-1108.

SUPPLEMENTAL FIGURES

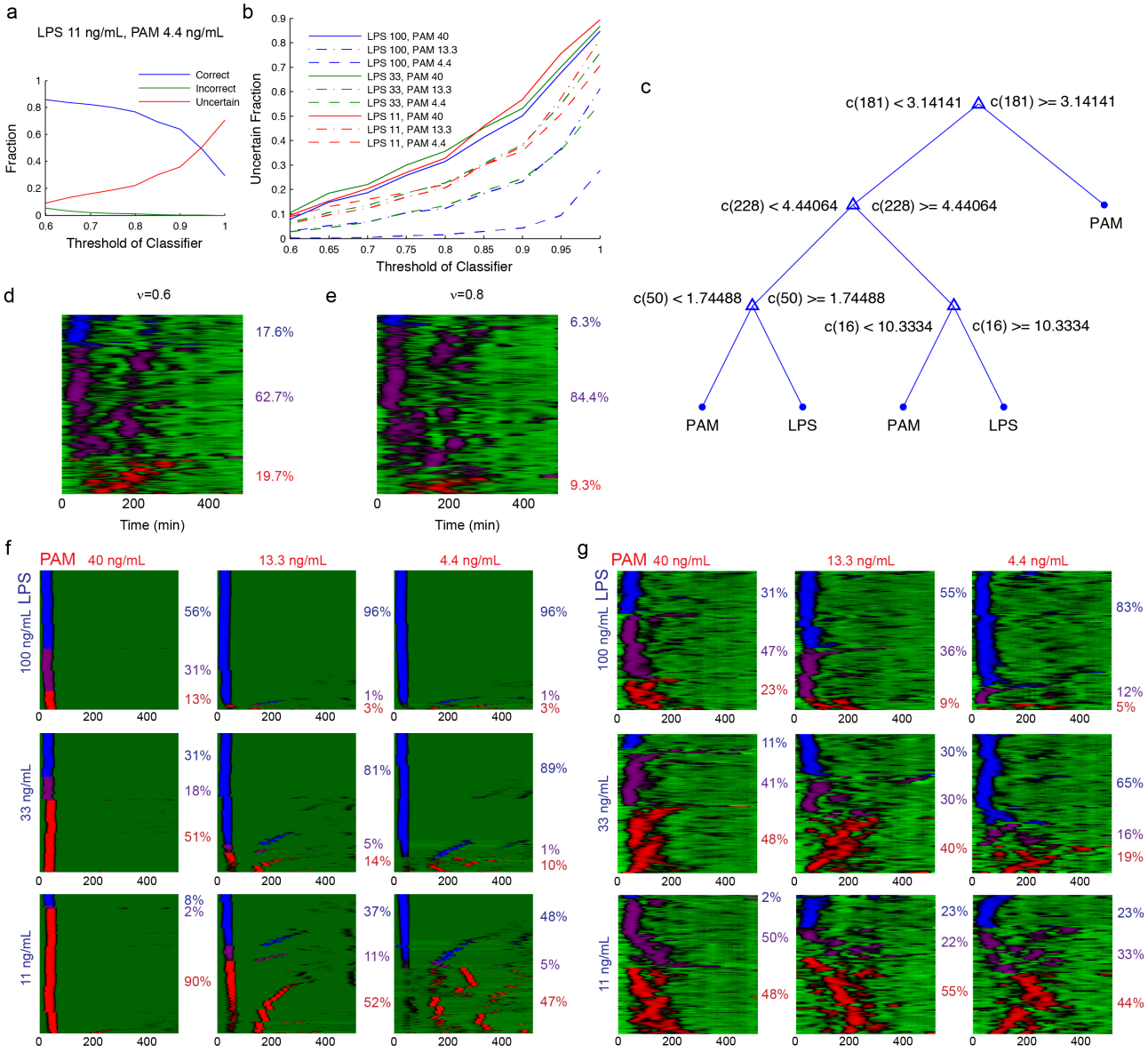

Figure S1. Evaluation of the classifier, related to Figure 1, 3 and 4. (a-b) The effects of the threshold ν on the accuracy of bagging classifiers. Each bagging classifiers contains 50 decision tree models. (a) For the input condition LPS 11 ng/mL and PAM 4.4 ng/mL, the fractions that the bagging classifiers output correct (blue), incorrect (green) and uncertain (red) labels as a function of threshold ν. (b) For all input conditions, the fractions that the bagging classifiers output uncertain labels as a function of threshold ν. (c) Example decision tree for LPS 11 ng/mL and PAM 4.4 ng/mL. The symbol c(t) represents the nuclear NF-κB concentration at *t* min after stimulation. (d-e) Classification of artificial "mixed" time courses. We restrict to the dose combination of LPS 11 ng/mL and PAM 4.4 ng/mL and create 1000 artificial "mixed" time courses by adding a randomly selected LPS-training trajectory and a randomly selected PAM-training trajectory. Classification of these artificial data is plotted for both (d) ν=0.6 and (e) ν=0.8. The percentages represent the fractions of LPS-like (blue), mixed (purple) and PAM-like (red) responses. (f-g) Classification with *N*=50

and ν=0.8. (f) Classification of model predicted cellular responses under co-stimulation, related to Figure 3D. (g) Classification of experimental cellular responses under co-stimulation, related to Figure 4B.

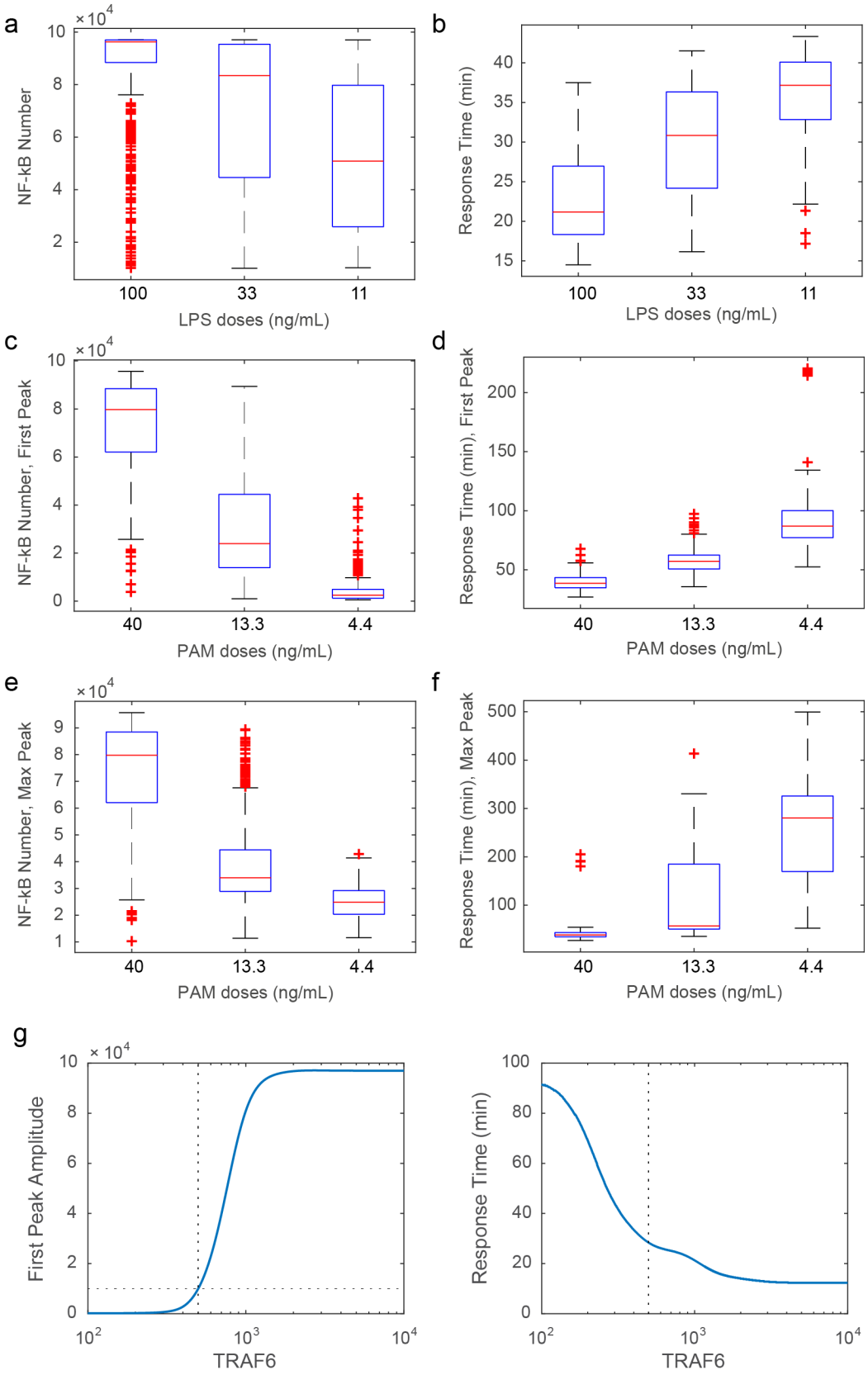

Figure S2. Model evaluation for one ligand, related to Figure 1 and 2. (a-f) Characteristics of simulated cellular responses stimulated by one ligand. (a-b) The characteristics of the first NF-κB peak under LPS stimulus; (c-d) The

characteristics of the first NF-κB peak under PAM stimulus; (e-f) The characteristics of the maximal NF-κB peak under PAM stimulus. (a,c,e) The distribution of the amplitudes of the NF-κB peaks. The total number of NF-κB in the cells is 10^5. (b,d,f) The distribution of the response times of the NF-κB peaks. 500 independent simulations are used to compute the distributions. Only active trajectories (more than 10% of NF-κB enters the cells) are considered. The model-predicted response times show good consistency with the experimental data, while the model produces a strong dependency between peak amplitudes and doses which is less strong in the experiments. (g) Relationship between a constant TRAF6a level and the properties of the first NF-κB peak. The dash line represents the threshold for activation.

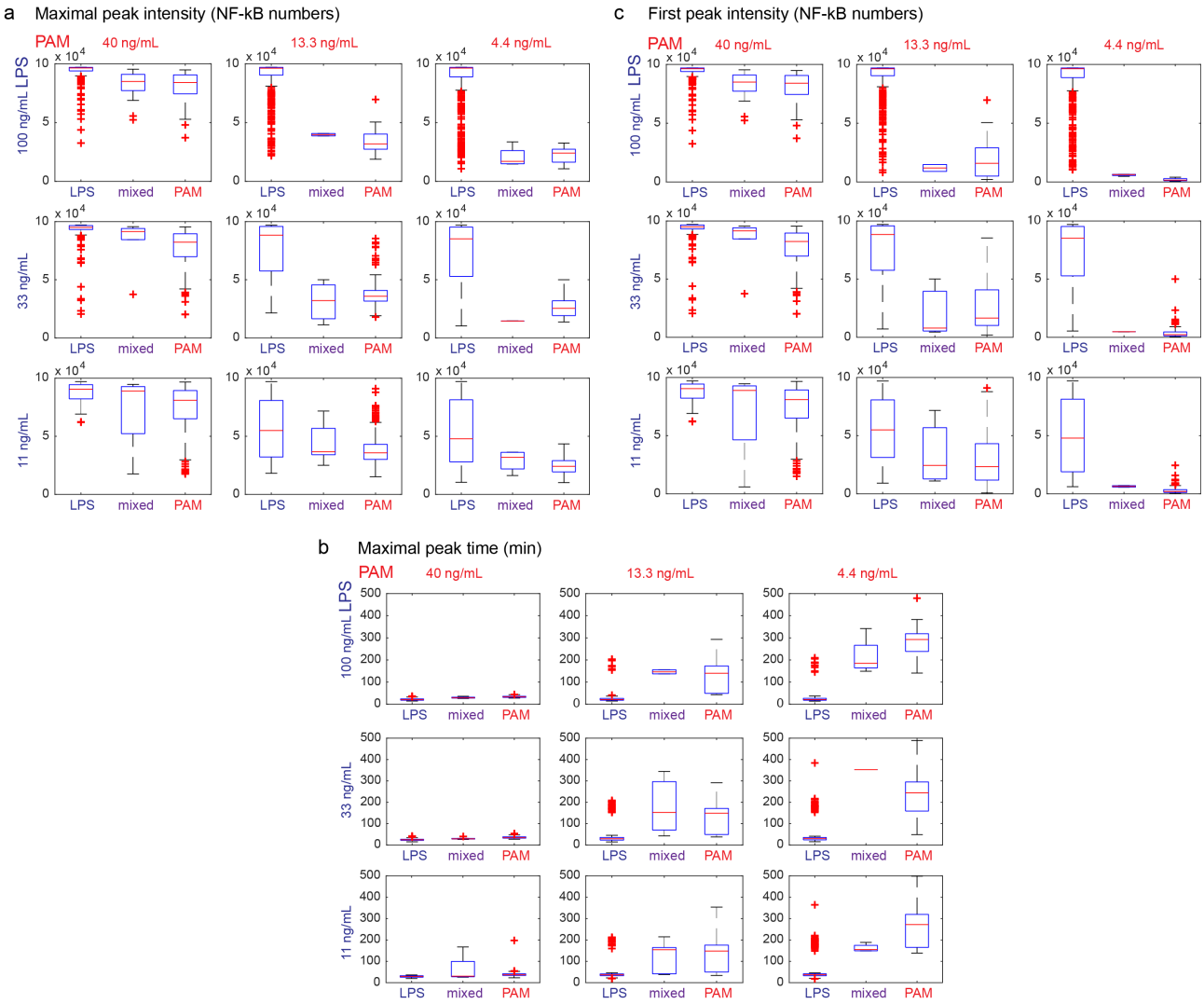

Figure S3. Model evaluation for co-stimulation, related to Figure 3. (a) Distribution of maximal NF-κB peak amplitudes. For each input condition, we simulate 500 trajectories and use classifier to classify all trajectories into LPS-like, PAM-like and mixed type. We then plot the distribution of the maximal peak amplitude for each category in the form of box plots. Only active trajectories are considered. Vertical axis represents the amplitude of the maximal peak in NF-κB numbers. The total number of NF-κB in the cells is 10^5. (b) Distribution of the maximal NF-κB peak response times. Vertical axis represents the response time of the maximal peak in minutes. (c) Distribution of the first NF-κB peak amplitudes. The characteristics for LPS-like and PAM-like trajectories generally show good agreement with cellular responses under single stimulation (Figure S2).

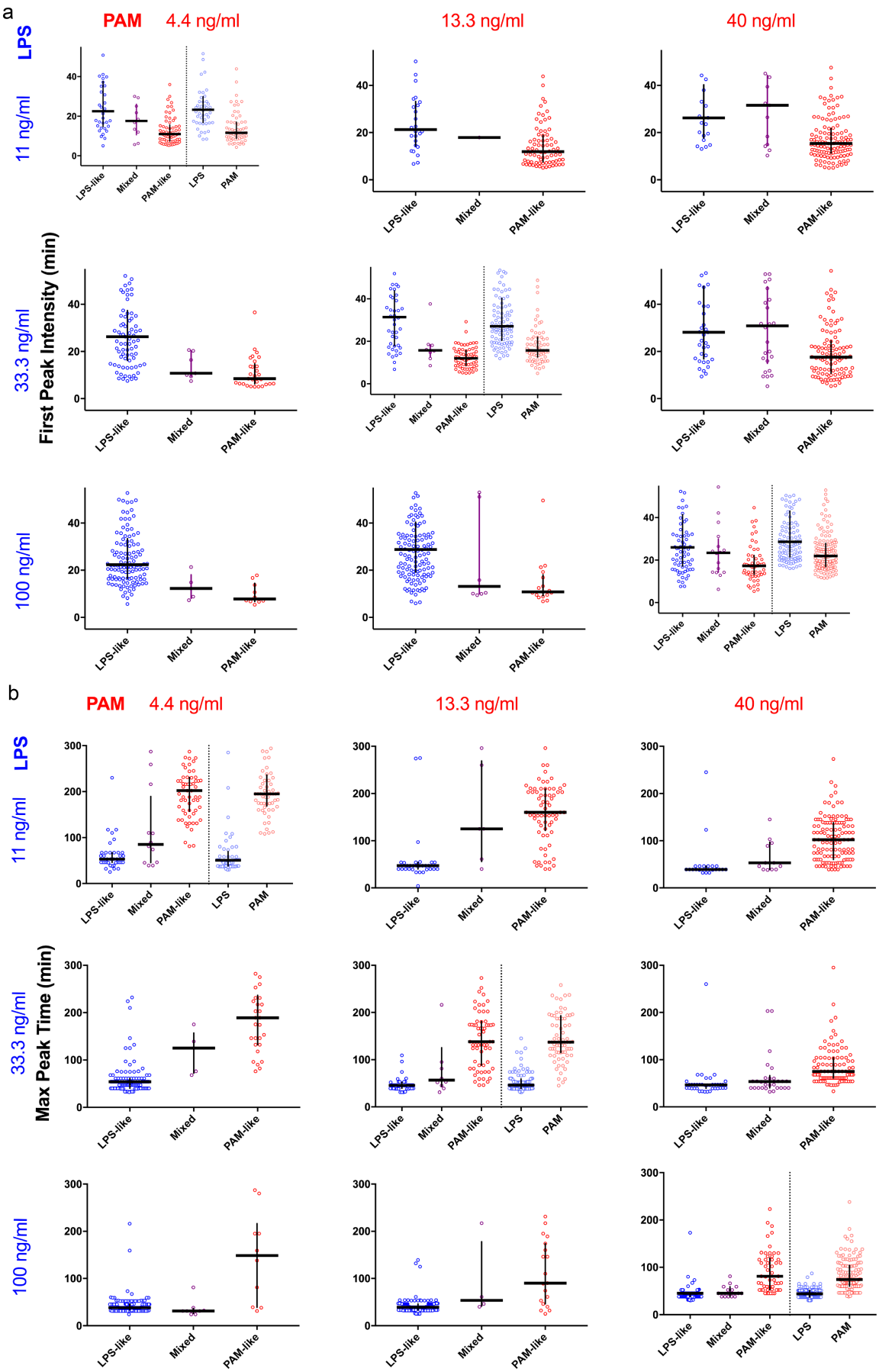
a
PAM
4.4 ng/ml
13.3 ng/ml
40 ng/ml
LPS
11 ng/ml
33.3 ng/ml
100 ng/ml
First Peak Intensity (min)
LPS-like
Mixed
PAM-like
LPS
PAM
b
Max Peak Time (min)

Figure S4. Evaluation of experimental cellular responses under co-stimulation, related to Figure 4. Experimental data are classified into “LPS-like”, “PAM-like” and “mixed” and plotted in the style of Figure 1C-D. We reproduce the data points in Figure 1C-D in “LPS” and “PAM” columns for comparison. (a) Distribution of first NF-κB peak amplitudes. Vertical axis represents the amplitude of the first peak in arbitrary units. The panel for LPS 11 ng/mL and PAM 4.4 ng/mL is reproduced from Figure 4D. (b) Distribution of maximal NF-κB peak response times. Vertical axis represents the response time of the maximal peak in minutes. The panel for LPS 11 ng/mL and PAM 4.4 ng/mL is reproduced from Figure 4E.

SUPPLEMENTAL TABLES

Table S1. The accuracy of the bagging classifiers, related to Figure 1.

	N=10	*N*=15	*N*=20	*N*=30	*N*=40	*N*=50
ν=0.60	0.90	0.89	0.89	0.89	0.89	0.89
ν=0.65	0.85	0.86	0.87	0.86	0.87	0.86
ν=0.70	0.85	0.83	0.85	0.84	0.84	0.84
ν=0.75	0.79	0.78	0.82	0.80	0.81	0.80
ν=0.80	0.79	0.78	0.77	0.77	0.77	0.77
ν=0.85	0.70	0.71	0.73	0.70	0.71	0.70
ν=0.90	0.70	0.62	0.66	0.64	0.64	0.63
ν=0.95	0.52	0.46	0.56	0.49	0.53	0.49
ν=1.00	0.52	0.46	0.41	0.36	0.32	0.30

Table S2. Quality assessment of the classifier for classifying single-stimulus time courses, related to Figure 1. N=50, ν=0.6. The quantities are evaluated by 10-fold CV. AUROC and AUPR are computed without the assignment of the uncertain label. The AUPR value is for reference only as the composition of the test data may vary in different CV runs. C, I and U stand for Correct, Incorrect and Uncertain labels.

Dose (LPS-PAM, ng/mL)	LPS responses			PAM responses			AUROC	AUPR
	C	I	U	C	I	U		
100-40	0.84	0.07	0.09	0.87	0.05	0.08	0.96	0.78
100-13.3	0.97	0.02	0.02	0.88	0.07	0.05	0.99	0.54
100-4.4	1.00	0.00	0.00	1.00	0.00	0.00	1.00	0.21
33-40	0.75	0.12	0.13	0.87	0.04	0.09	0.95	0.75
33-13.3	0.90	0.05	0.05	0.83	0.09	0.08	0.97	0.66
33-4.4	0.95	0.04	0.01	0.95	0.01	0.03	0.99	0.37
11-40	0.59	0.20	0.21	0.94	0.01	0.06	0.93	0.63
11-13.3	0.84	0.10	0.06	0.89	0.06	0.05	0.97	0.64
11-4.4	0.83	0.08	0.09	0.89	0.02	0.09	0.98	0.57

Table S3. Statistics of the example decision tree, related to Figures 1 and S1.

Split	Importance	LPS labels to classify	PAM labels to classify
c(181)	0.0851	48	60
c(228)	0.0220	48	10
c(50)	0.0058	46	2
c(16)	0.0074	2	8

Table S4. Mathematical model, related to Figure 2.

TLR4-mediated signaling		TLR2-mediated signaling	
$LPS \rightarrow \emptyset$	Degradation of LPS	$PAM \rightarrow \emptyset$	Degradation of PAM
$l_d[LPS]$		$p_d[PAM]$	
$LPS + TLR4 \rightarrow LPS.TLR4$	Binding of LPS and TLR4	$PAM + TLR2 \rightarrow PAM.TLR2$	Binding of PAM and TLR2
$l_b[LPS][TLR4]$		$p_b[PAM][TLR2]$	
$LPS.TLR4 \rightarrow LPS + TLR4$	Unbinding of LPS and TLR4	$PAM.TLR2 \rightarrow PAM + TLR2$	Unbinding of PAM and TLR2
$l_f[LPS.TLR4]$		$p_f[PAM.TLR2]$	
$TRAF6 \rightarrow TRAF6a(LPS)$	Activation of TRAF6a by LPS.TLR4	$TRAF6 \rightarrow TRAF6a(PAM)$	Activation of TRAF6a by PAM.TLR2
$l_a[LPS.TLR4][TRAF6] * \frac{k_{M,A20(LPS)}}{k_{M,A20(LPS)} + [A20]} \frac{k^4_{M,miR146a(LPS)}}{[miR146a]^4 + k^4_{M,miR146a(LPS)}}$		$p_a[PAM.TLR2][TRAF6] * \frac{k_{M,A20(PAM)}}{k_{M,A20(PAM)} + [A20]} \frac{k^4_{M,miR146a(PAM)}}{[miR146a]^4 + k^4_{M,miR146a(PAM)}}$	
$TRAF6a(LPS) \rightarrow TRAF6$	Inactivation of TRAF6a	$TRAF6a(PAM) \rightarrow TRAF6$	Inactivation of TRAF6a
$l_i[TRAF6a(LPS)]$		$p_i[TRAF6a(PAM)]$	
miR-146a related signaling			
$MIR146A\ gene\ off \rightarrow on$		Activation of the MIR146a gene	
$g_{1,miR146a}[NF\kappa B.nuc][miR146a\ gene\ off]$			
$MIR146A\ gene\ on \rightarrow off$		Inactivation of the MIR146a gene	
$g_{2,miR146a}[I\kappa B\alpha.nuc][miR146a\ gene\ on]$			
$\emptyset \rightarrow miR-146a$		Synthesis of miR-146a	
$g_{tsc,miR146a}[miR146a\ gene\ on]$			
$miR-146a \rightarrow \emptyset$		Degradation of miR-146a	
$d_{,miR146a}[miR146a]$			

Table S5. Parameter values, related to Figure 2.

TLR4-mediated signaling		TLR2-mediated signaling	
μ_l	Mean parameter of TLR4 distribution	μ_p	Mean parameter of TLR2 distribution
8.0	(Kellogg et al., 2015)	8.0	Assume same as LPS pathway
σ_l	Standard deviation parameter of TLR4 distribution	σ_p	Standard deviation parameter of TLR2 distribution
0.8	(Kellogg et al., 2015)	0.4	Fitted
l_d	Degradation rate of LPS	p_d	Degradation rate of PAM
$5*10^{-4}$	(Kellogg et al., 2015)	$1*10^{-5}$	Fitted
l_b	Binding rate between LPS and TLR4	p_b	Binding rate between PAM and TLR2
$1*10^{-9}$	Fitted	$5*10^{-11}$	Fitted
l_f	Unbinding rate between LPS and TLR4	p_f	Unbinding rate between PAM and TLR2
$5*10^{-4}$	Rounded from (Kellogg et al., 2015)	$1*10^{-6}$	Fitted
l_a	Activation rate of TRAF6 by LPS.TLR4	p_a	Activation rate of TRAF6 by PAM.TLR2
$1*10^{-7}$	(Kellogg et al., 2015)	$1*10^{-7}$	Assume same as LPS pathway
$k_{M,A20(LPS)}$	Michaelis-Menten constant for the inhibitory effect of A20	$k_{M,A20(PAM)}$	Michaelis-Menten constant for the inhibitory effect of A20
10^5	(Kellogg et al., 2015)	10^5	Assume same as LPS pathway
$k_{M,miR146a(LPS)}$	Hill constant for the inhibitory effect of miR-146a	$k_{M,miR146a(PAM)}$	Hill constant for the inhibitory effect of miR-146a
$6*10^2$	Fitted	$6*10^2$	Assume same as LPS pathway
l_i	Inhibition rate of TRAF6a(LPS)	p_i	Inhibition rate of TRAF6a(PAM)
$1*10^{-2}$	(Kellogg et al., 2015)	$1*10^{-2}$	Assume same as LPS pathway
$c_{1(LPS)}$	Activation rate of IKK by TRAF6a(LPS)	$c_{1(PAM)}$	Activation rate of IKK by TRAF6a(PAM)
$2*10^{-2}$	(Kellogg et al., 2015)	$2*10^{-2}$	Assume same as LPS pathway
$K_{TRAF6a(LPS)}$	Hill constant for the activation of IKK by TRAF6a(LPS)	$K_{TRAF6a(PAM)}$	Hill constant for the activation of IKK by TRAF6a(PAM)
$3.5*10^3$	(Kellogg et al., 2015)	$3.5*10^3$	Assume same as LPS pathway
miR-146a related signaling			
$g_{1,miR146a}$	Activation rate of MIR146A genes	$1*10^{-7}$	Fitted
$g_{2,miR146a}$	Inactivation rate of MIR146A genes	$2*10^{-6}$	Fitted
$g_{tsc,miR146a}$	Synthesis rate of miR-146a	0.5	Fitted
$d_{miR146a}$	Degradation rate of miR-146a	$2*10^{-5}$	Assume 5 h half-life, support from (Yao et al., 2012)

Table S6. Fraction of active cells of the simulated and experimentally measured cellular responses, related to Figure 1-4.

Input Condition	Experimental Trajectories	Simulated Trajectories
LPS 100 ng/mL	0.95	0.974
LPS 33 ng/mL	0.73	0.852
LPS 11 ng/mL	0.47	0.472
PAM 40 ng/mL	1.00	1.000
PAM 13.3 ng/mL	1.00	1.000
PAM 4.4 ng/mL	1.00	0.950
LPS 100 ng/mL, PAM 40 ng/mL	1.00	1.000
LPS 100 ng/mL, PAM 13.3 ng/mL	1.00	1.000
LPS 100 ng/mL, PAM 4.4 ng/mL	1.00	0.998
LPS 33 ng/mL, PAM 40 ng/mL	1.00	1.000
LPS 33 ng/mL, PAM 13.3 ng/mL	1.00	1.000
LPS 33 ng/mL, PAM 4.4 ng/mL	1.00	0.996
LPS 11 ng/mL, PAM 40 ng/mL	1.00	1.000
LPS 11 ng/mL, PAM 13.3 ng/mL	1.00	1.000
LPS 11 ng/mL, PAM 4.4 ng/mL	1.00	0.982

Table S7. The fraction of LPS-, PAM- and mixed-type responses, related to Figure 3D.

Input Condition	LPS	PAM	Uncertain
LPS 100 ng/mL, PAM 40 ng/mL	83%	14%	4%
LPS 100 ng/mL, PAM 13.3 ng/mL	96%	4%	0%
LPS 100 ng/mL, PAM 4.4 ng/mL	96%	3%	0%
LPS 33 ng/mL, PAM 40 ng/mL	34%	53%	14%
LPS 33 ng/mL, PAM 13.3 ng/mL	83%	15%	1%
LPS 33 ng/mL, PAM 4.4 ng/mL	89%	10%	0%
LPS 11 ng/mL, PAM 40 ng/mL	8%	91%	1%
LPS 11 ng/mL, PAM 13.3 ng/mL	42%	56%	2%
LPS 11 ng/mL, PAM 4.4 ng/mL	51%	48%	1%

Table S8. Statistical analysis comparing NF-κB peak characteristics under co-stimulation, related to Figure 4. For all dose combinations, first peak intensity and maximum peak time are statistically different between "LPS-like" and "PAM-like" classes by Mann-Whitney test.

Input Condition	**First Peak Intensity** *LPS-like vs. PAM-like (p value)*	**Max Peak Time** *LPS-like vs. PAM-like (p value)*
LPS 100 ng/mL + PAM 40 ng/mL	<0.0001	<0.0001
LPS 100 ng/mL + PAM 13.3 ng/mL	<0.0001	<0.0001
LPS 100 ng/mL + PAM 4.4 ng/mL	<0.0001	0.011
LPS 33 ng/mL + PAM 40 ng/mL	<0.0001	<0.0001
LPS 33 ng/mL + PAM 13.3 ng/mL	<0.0001	<0.0001
LPS 33 ng/mL + PAM 4.4 ng/mL	<0.0001	<0.0001
LPS 11 ng/mL + PAM 40 ng/mL	<0.0001	<0.0001
LPS 11 ng/mL + PAM 13.3 ng/mL	<0.0001	<0.0001
LPS 11 ng/mL + PAM 4.4 ng/mL	<0.0001	<0.0001

Table S9. Statistical analysis of comparing NF-κB peak characteristics of classified as LPS-like (PAM-like) under co-stimulation to LPS (PAM) alone, related to Figure 4. In all cases there is *not* a significant difference in first peak intensity and maximum peak time in cells classified as LPS-like (PAM-like) under co-stimulation compared to LPS (PAM) stimulation alone.

Input Condition	**First Peak Intensity (p value)** *LPS-like vs. LPS*	**Max Peak Time (p value)** *PAM-like vs. PAM*
LPS 100 ng/mL + PAM 40 ng/mL	0.4543	0.8295
LPS 33 ng/mL + PAM 13.3 ng/mL	0.2064	0.9593
LPS 11 ng/mL + PAM 4.4 ng/mL	0.1545	0.8273